Supporting information

Double-shelled Cu_2O/MnO_x Mesoporous Hollow Structure for CO_2 Photoreduction with Enhanced Stability and Activity

Hailing Huo,[a] Dong Liu,[b] Hao Feng,[b] Zhihong Tian,[c] Xuan Liu,[d] and Ang Li *[d]

[a] *School of Chemical and Environmental Engineering, Shanxi Datong University, Xingyun street 405, Datong, Shanxi, China 037009*
[b] *School of Energy and Power Engineering, Nanjing University of Science and Technology, Xiaolingwei street 200, Nanjing, Jiangsu, China 210094*
[c] *Key Laboratory of Materials Processing and Mold (Zhengzhou University), Ministry of Education, National Engineering Research Center for Advanced Polymer Processing Technology, Zhengzhou University, Zhengzhou, Henan, China 450002*
[d] *Department of Applied Physics, School of Science, Nanjing University of Science and Technology, Xiaolingwei street 200, Nanjing, Jiangsu, China 210094*

*Email: liang2100@njust.edu.cn

Experimental Procedures

Materials

$CuSO_4 \cdot 5H_2O$ (99%) and ascorbic acid (>99.7%) were purchased from Sinopharm. Cetyltrimethylammonium bromide (CTAB) (>99%) and ethanol were purchased from Guangfu. $KMnO_4$ (99%) was purchased from Jiangtian. NaOH (≥99%) was purchased from Kemiou. Na_2SO_3 (99%) was purchased from Yuanli. $KHCO_3$ (99.5%) was purchased from Macklin. Deionized water (18.25 MΩ·cm) supplied by a UP Water Purification System was used in the whole experimental processes. All chemicals were obtained from commercial suppliers and used without further purification. FTO substrates (F:SnO_2, 14 Ω per square) were purchased from Nippon Sheet Glass, Japan. And before using, the FTO substrates were ultrasonically cleaned for 20 minutes each in deionized water, ethanol, and acetone, respectively.

Characterization

Transmission electron microscope (TEM) was performed on a JEOL JEM 2100F electron microscope. Crystalline structures were evaluated by XRD analysis using a Bruker D8 Focus operating at 40 kV and 40 mA equipped with a nickel-filtered Cu Kα radiation ($\lambda = 1.54056$ Å). BET surface area and pore structure of catalysts were measured using a Micromeritics Tristar 3000 analyzer by nitrogen adsorption at 77 K. The specific surface areas were calculated from the isotherms using the BET method. The pore distribution and the cumulative volumes of pores were obtained by the BJH method from the desorption branch of the adsorption isotherms. PL spectra were performed on Hitachi F-4600 fluorescence spectrophotometer. Light absorption spectra were recorded using a Hitachi u-4100 UV/Vis under the visible light of 400-800 nm.

Methods

Section 1. Synthesis of single-shelled Cu_2O hollow structure (S-CH). A soft-template method was adopted using CTAB as the template for the preparation of S-CH. $CuSO_4 \cdot 5H_2O$ (0.05 g) was dispersed in 100 mL of CTAB solution (0.13 M). After stirring for 5 minutes, it should be kept static for 10 minutes to ensure that Cu^{2+} was fully adsorbed. Then 0.18 g of ascorbic acid was added. Next, the solution was heated at 60℃ for 20 minutes. Afterwards, 10 mL of NaOH solution (0.2 M) was added dropwise and stirred for 10 minutes. Then the precipitates obtained were separated by centrifugation, washed twice with deionized water and ethanol and vacuum dried at 50°C for 5 h.

Section 2. Synthesis of double-shelled Cu_2O hollow structure (D-CH). The synthetic process of D-CH was similar to the synthesis of S-CH. The difference was that the concentration of CTAB was increased from 0.13 M to 0.15 M.

Section 3. Synthesis of single-shelled Cu_2O/MnO_x hollow structure (S-CMH). $KMnO_4$ (0.02 g) was dispersed in 100 mL of CTAB solution (0.13 M) and stirred for 5 minutes. Then it should be kept static for 10 minutes, making MnO_4^- in solution exchange with Br^- (came from CTAB) adequately. Afterwards, $CuSO_4 \cdot 5H_2O$ (0.05 g) was added and stirred for 5 minutes, and then it should be still kept static for 10 minutes to ensure that Cu^{2+} was fully adsorbed. Then 50 mL of ethanol, which acted as the reductant to produce MnO_x from MnO_4^- and Cu_2O from Cu^{2+}, was injected to the solution. Subsequently, the solution was heated at 60℃ for 20 minutes. Next, 10 mL NaOH solution (0.2 M) was added dropwise and stirred for 10 minutes. Finally, the precipitates obtained were separated by centrifugation, washed twice with deionized water and ethanol and vacuum dried at 50°C for 5 h.

Section 4. Synthesis of double-shelled Cu_2O/MnO_x hollow structure (D-CMH). The synthetic process of D-CMH was similar to the synthesis of S-CMH. The difference was still that the concentration of CTAB was increased from 0.13 M to 0.15 M.

Section 5. Synthesis of benchmark Cu_2O nanoparticles (CP). The synthetic process of CP was similar to the synthesis of S-CH. The difference was that CTAB was not added to the solution in the synthetic process of CP.

Section 6. CO_2 photoreduction. The home-made photocatalytic reactor was composed of a sealed chamber, an embedded window made by quartz glass and a liquid sampling port sealed by silicone pad. The reactor was connected to a gas circulation system with a ten-port value (VICI) for on-line sampling to a gas chromatograph (GC, Ruimin GC 2060, Shanghai). The gas circulation system was primarily made of stainless-steel tubing and a customized mechanical circulation pump for gas circulation. The mechanical pump was connected into the system to exhaust the carrier gas of the gas chromatograph when switching back the ten-port value. A pressure gauge was also connected to the system to monitor the pressure. The total volume of the gas in the circulation system after filling the reactor with solvent was 80 mL. Measurable tube (1 mL) of GC was also involve in this closed system. The ratio of total volume for gas in the circulation system to the volume of measurable tube was defined as the volume factor.

Before the start of reaction, catalysts (0.05g) were mixed with 40 mL $KHCO_3$ (0.1 M, to enhance the solubility of CO_2) and Na_2SO_3 (0.1 M, acting as holes sacrifice agent) aqueous solution in the reactor, then the system was evacuated to remove air. Subsequently, the suspension in reactor was purged with CO_2 ($\geq$ 99.995%) for 1 h to achieve CO_2 saturation and the initial CO_2 pressure was kept at atmospheric pressure. There was no more CO_2 purged into the closed system during the reaction. The gases in the closed circulation system were continuously circulated through the suspension for the entire reaction period. The reactions were carried out under visible light irradiation ($\lambda > 420$ nm, 80 mW cm^{-2}). The visible light was provided by a 300 W Xenon lamp and a filter cut 420 (Perfectlight co. ltd.). After 1 h of irradiation, gas in measurable tube was injected into the GC by switching back the ten-port value for analysis. The amount of generation for every component during 1 h was the generation rate, meaning product generation during unit time. To avoid the error caused by the volume change and gas leakage during the switch of value, after the irradiation, the catalysts were separated by centrifugation and used for another 1 h following similar operation process. After three times, the average value and standard deviation of the results were exhibited as the production rate and error bar.

The analyses of the gaseous reaction mixtures containing CO, CH_4, H_2 were carried out using a gas chromatograph, which was equipped with a TCD, an FID and a mechanizer which contained Ni catalyst. Argon ($\geq$ 99.999%) was used as the carrier gas. The back channel of GC was equipped with two packed columns, TDX-01 and Molsieve 5 Å, and two gas switching valves. During the analysis, 1.0 mL of gas sample in the sample loop of ten-port value was introduced to the TDX-01 column where CO_2 was separated from the other gases due to its longer retention time. The rest of the gases after the TDX-01 column was further separated by the Molsieve 5 Å column. The gas product of H_2 was detected by TCD and CH_4, CO were further detected by FID with higher sensitivities. The role of mechanizer was to convert CO to CH_4 for FID analysis. External standard method was used to calculate the amount of every component from the peak area of GC. Specifically, gas of known amount was injected into GC and the peak area of every amount was recorded, which could be used to make a standard table to exhibit the relationship between area peaks and product amounts by data fitting. Based on the relationship, we can calculate the amount of every component from the peak area of GC. The stability test was carried out by prolonging the reaction time to 10 hours and recording the activity every 2 hours.

Section 7. Mott-Schottky plots for Cu_2O and MnO_x. Pure Cu_2O and MnO_x with the similar forming-manners of D-CMH were needed for the measurements of Mott-Schottky plots to prove which type of semiconductors the Cu_2O shells and the loaded MnO_x belonged to. Pure Cu_2O (D-CH) was synthesized by the method introduced in **Section 2**. Pure MnO_x was synthesized by a method similar to **Section 4** without the adding of $CuSO_4 \cdot 5H_2O$. In detail, 0.10 g $KMnO_4$ was dispersed in 100 mL CTAB solution (0.15 M) and stirred for 5 minutes, then kept static for 10 minutes. Subsequently, 50 mL ethanol, acting as the reductant to produce

MnO_x from MnO_4^-, was injected to the solution. Then the solution was heated at 60℃ for 20 minutes. After that, 10 mL NaOH solution (0.2 M) was added dropwise and stirred for 10 minutes, and pure MnO_x was synthesized. Since the synthetic processes of pure MnO_x and the MnO_x in D-CMH were the same, their properties should be also the same to each other. Then the as-synthesized pure Cu_2O and pure MnO_x were droplet coated on conductive glasses (FTO) uniformly for the further tests of Mott-Schottky plots, respectively. The Mott-Schottky plots were measured in a 0.5 M KPi buffer (pH 7) at a frequency of 1000 Hz and amplitude of 10 mV under the dark condition. The measured potentials *vs.* Ag/AgCl were converted to the reversible hydrogen electrode (RHE) scale according to the Nernst equation: $E_{\mathrm{RHE}} = E_{\mathrm{Ag/AgCl}} + 0.059 \times \mathrm{pH} + 0.1976$.[1]

Section 8. Synthesis of Cu_2O/MnO_x hollow structure by impregnation method (I-Cu_2O/MnO_x). To further investigate the influences of different MnO_x loading methods, Cu_2O/MnO_x hollow structure by impregnation method was synthesized as a comparison. Cu_2O hollow structure was firstly synthesized according to the **Section 1** of method in supporting information, and then impregnated in 50 mL $KMnO_4$ solution (0.2 g L^{-1}) with stirring for 30 minutes. Then ethanol was added as reducing agent, and 5 mL NaOH solution (0.2 M) was added to provide alkaline surrounding.

The formation of hollow structures is based on a soft-template method, using surfactant CTAB as the template. Surfactant molecules can self-assemble in solution, forming different structures under different conditions. The final structure of the product obtained is closely related to the aggregate structure formed by the surfactant.

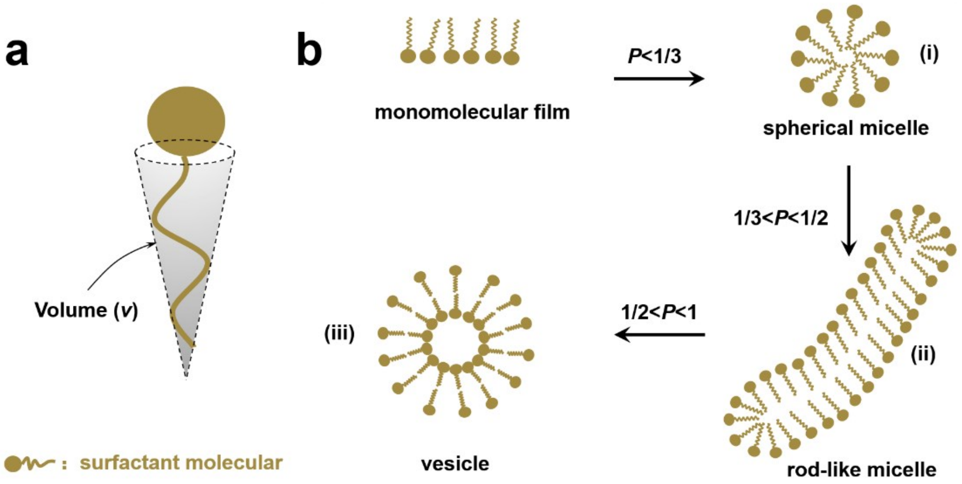

Fig. S1 (a) The schematic diagram of volume parameter (v) for packing parameter (P), (b) Packing parameter (P) of surfactant molecules and preferred aggregate structures for geometrical packing reasons.

Packing parameter (P), the ratio $v/(la)$, is seen to be very useful when discussing the type of structure formed by surfactant molecules in terms of geometrical analysis. That is to say $P= v/(la)$, where v, l and a are parameters of a surfactant molecule, and also v and a can vary with different conditions, such as surfactant concentrations, inorganic additives, temperatures and so on. Specifically, v is the volume of one chain (the hydrophobic part of a surfactant molecule) (Fig. S1a). l is the length of the extended alkyl chain. a is the cross-sectional area of one surfactant molecule.[2, 3]

When $P<1/3$, spherical micelles are dominant (Fig. S1b (i)). The range of P value is 1/3-1/2 and rod-like micelle structures are characteristic (Fig. S1b (ii)).[2, 3] If it is between 1/2 and 1, surfactant molecules will self-assemble into vesicles (Fig. S1b (iii)).[3] Thus, under appropriate conditions, micelles can be transformed into vesicles.

Moreover, for aqueous solution, in a micelle the surfactant hydrophobic group is directed towards the interior of the cluster and the hydrophilic polar head group is outside, directing towards the exterior aqueous solution. Similarly, the outermost part of the vesicle is also composed of hydrophilic groups.[4, 5]

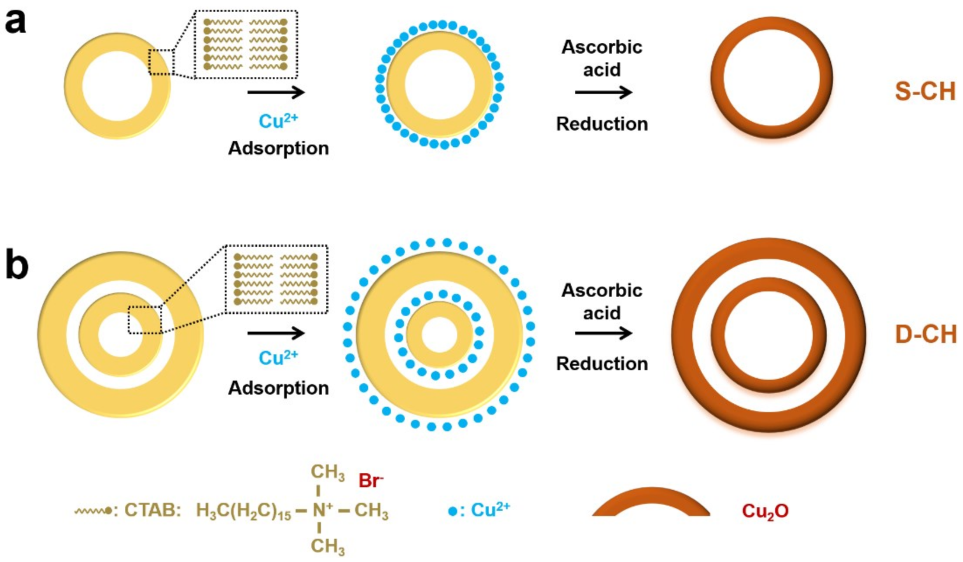

Fig. S2 Formation processes for single-shelled Cu_2O hollow structure (S-CH) (a) and double-shelled Cu_2O hollow structure (D-CH) (b) in the presence of different CTAB templates.[6]

It has been proved that the concentration of surfactants can change the morphology of as-formed templates from micelles to vesicles and multi-lamellar vesicles.[7] Actually, by adjusting the concentration of CTAB to 0.13 M whilst keeping the other conditions constant, CTAB molecules could aggregate to form single-lamellar vesicles. Thus, actually single-lamellar CTAB vesicles were the real templates for the formation of single-shelled hollow structures (Fig. S2a). However, as the concentration of CTAB increased to 0.15 M, double-lamellar vesicles were characteristic. So, in fact, the double-lamellar CTAB vesicles were the templates for the formation of double-shelled hollow structures (Fig. S2b).

In the synthetic processes of Cu_2O hollow structures, because of the ionization of CTAB hydrophilic segment, Br^- would be exposed to form the negative charged interface on the hydrophilic part, outside of vesicles, whether the vesicles were single-lamellar or double-lamellar. Then Cu^{2+} could be adsorbed on the hydrophilic end to form Cu-Br moieties by electrostatic interaction, which leaded to enrichments of Cu^{2+} at the interface. Then Cu^{2+} was reduced to Cu_2O by reducing agent and the soft template CTAB was entirely removed by washing with deionized water and ethanol several times, forming Cu_2O hollow structures (Fig. S2). It should be noted that since the structures of the vesicle templates were sensitive to many parameters (temperature, pH value, inorganic additives, ionic strength, etc.), the other conditions should be kept constant whilst adjusting the concentration of CTAB.[6] For instance, if the temperature was changed, different results would be obtained. Relevant TEM images were shown in Fig. S3.

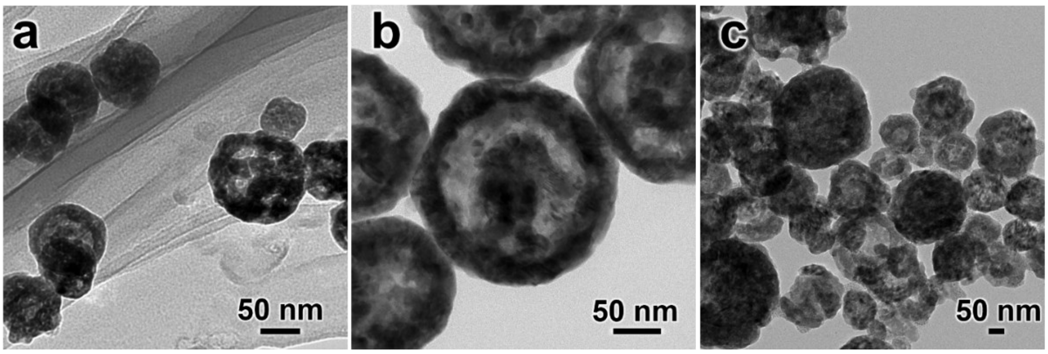

Fig. S3 TEM images of products obtained at different temperatures. (a) 40℃, (b) 60℃, (c) 80℃

It could be seen that when the temperature was lower (Fig. S3a), very few products could be obtained and no obvious double-shelled hollow structures could be observed. However, if the temperature was raised to an appropriate value, such as 60℃ (Fig. S3b), uniform double-shelled hollow structures could be successfully synthesized. But if the temperature was higher (Fig. S3c), double-shelled hollow structures almost disappeared and the sizes of products were clearly non-uniform, which was unwanted.

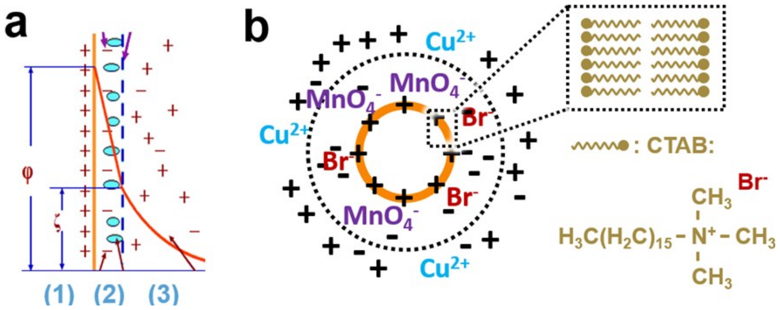

Fig. S4 (a) Modified adsorption mode. (b) Vesicle after the adding of MnO_4^- and Cu^{2+}.

According to the theory of modified adsorption model, a charged surface (Fig. S4a (1)) always adsorbs a layer of opposite electric charge (Fig. S4a (2)), then followed by a small amount of charge with the same electricity as the charged surface due to electrostatic interaction (Fig. S4a (3)). Thus, when CTAB vesicle was formed in solution (Fig. S4b), because of its ionization, it could appear a charged surface with positive charge of N^+. Then Br^- would be exposed to form the negative charged surface next to the positive charged surface of N^+. When $KMnO_4$ and $CuSO_4$ were added to the solution, MnO_4^- in solution would exchange with Br^- partially, and Cu^{2+} would be adsorbed on the negative charged surface because of electrostatic interaction. After the adding of ascorbic acid, MnO_4^- and Cu^{2+} were reduced together to form MnO_x and Cu_2O. Then Cu_2O hollow structure loaded with MnO_x was formed.

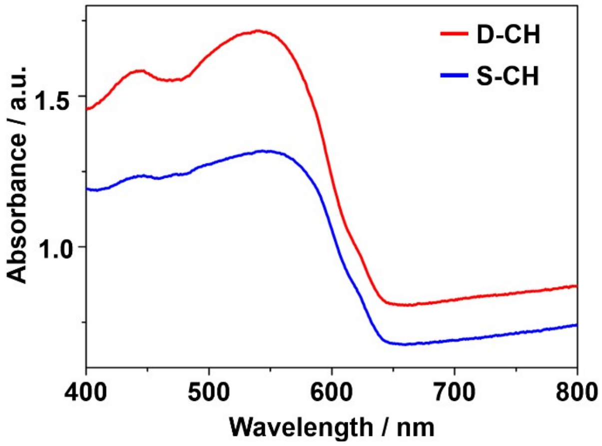

Fig. S5 Light absorption spectra of D-CH and S-CH.

The absorption edges of double-shelled Cu_2O hollow structure (D-CH) and single-shelled Cu_2O hollow structure (S-CH) are the same. However, the light absorption intensity of D-CH is much higher than S-CH, illustrating the better light absorption property of D-CH than S-CH, which is desired for photocatalyst.

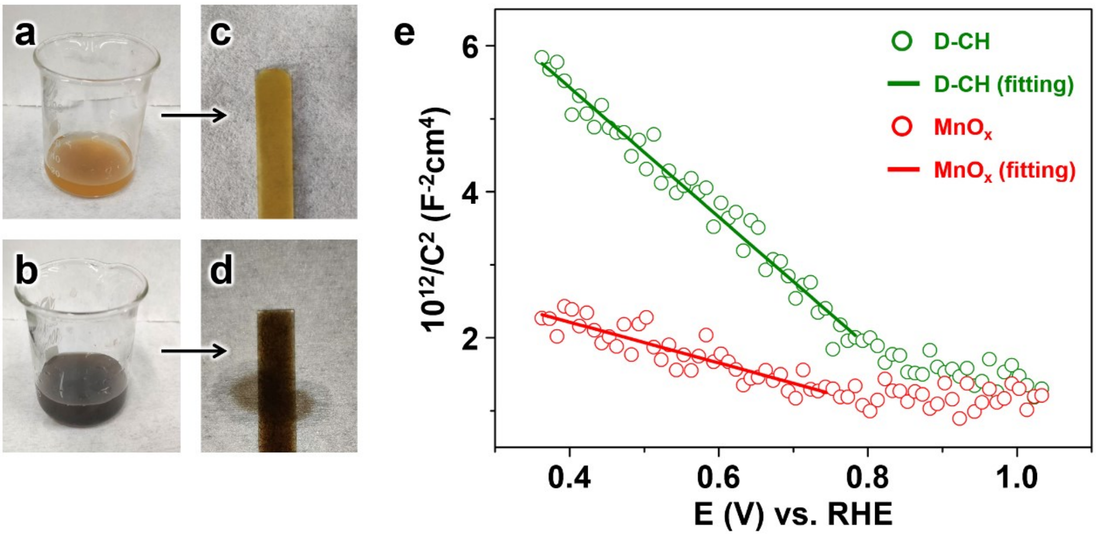

Fig. S6 Pure Cu_2O (D-CH) and pure MnO_x synthesized and the results of Mott-Schottky plots. (a) pure Cu_2O (D-CH), (b) pure MnO_x, (c, d) Pure Cu_2O (D-CH) and pure MnO_x were uniformly droplet coated on the conductive glasses (FTO), respectively. (e) Mott-Schottky plots of pure Cu_2O (D-CH) and pure MnO_x.

The measurement processes of Mott-Schottky plots were introduced in **Section 7** of the method in supporting information. As the results shown in Fig. S6e, for both Cu_2O and MnO_x the negative slopes of Mott-Schottky plots can be observed, indicating both the Cu_2O and MnO_x synthesized here are p-type semiconductors,[1, 8, 9] which could be further supported by published results.[8, 10] Thus, there is no p-n junction between the Cu_2O shells and the loaded MnO_x. The mechanism of property enhancement by controlled growth of MnO_x on the as-synthesized Cu_2O hollow structures may be attributed to the energy band mechanism of MnO_x, which is good at trapping holes from appropriate semiconductors.[11-13]

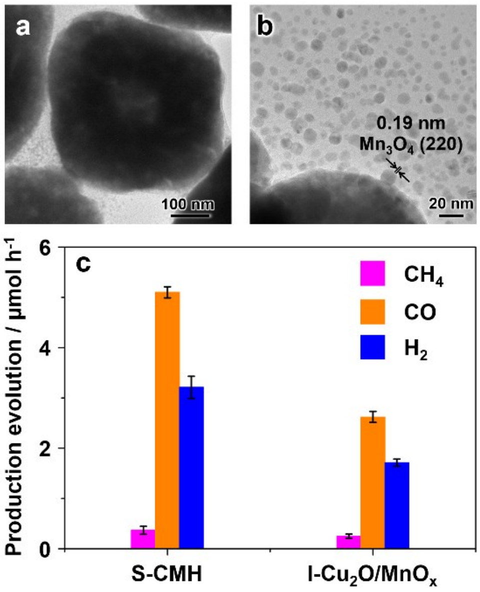

Fig. S7 TEM image (a) and HRTEM image (b) of Cu_2O/MnO_x hollow structure synthesized by impregnation method (I-Cu_2O/MnO_x), and photoactivities of S-CMH and I-Cu_2O/MnO_x (c).

Systematically investigating and comparing the way of how the growth of MnO_x on Cu_2O would be useful to understand how MnO_x influenced the photocatalytic activity. In this work, ethanol was used as a week reducing agent to simultaneously form Cu_2O and MnO_x from Cu^{2+} and MnO_4^-, respectively (see **Section 3** and **Section 4** of method in supporting information). Because of the alkaline surrounding, the oxidability of MnO_4^- was restrained to some extent. Thus, MnO_x could be formed slowly and uniformly (Fig. 3). Also, since MnO_x was in-situ formed on Cu_2O simultaneously, the interaction between them was strong, which was beneficial to charge transfer.[14] To illustrate the advantages of the MnO_x loading method used for S-CMH and D-CMH in this work, as a comparison we then adopted the traditional impregnation method to synthesize Cu_2O/MnO_x hollow structure (denoted as I-Cu_2O/MnO_x) (Fig. S7a, b). The synthetic process was shown in **Section 8** of method in supporting information. Compared with S-CMH (Fig. 3a and b), I-Cu_2O/MnO_x showed a thicker shell (Fig. S7a). Furthermore, it could be observed that lots of MnO_x particles were dissociated with Cu_2O (Fig. S7b), which could not trap holes and promote oxidation reactions. Also, compared with S-CMH, I-Cu_2O/MnO_x showed the poorer photoactivity (Fig. S7c), indicating the strong connection of Cu_2O and MnO_x was desired for photocatalysis. Thus, it could be concluded that the different ways of MnO_x growing on Cu_2O could affect the photocatalytic activity by influencing the interaction between Cu_2O and MnO_x.

References

1. X. Chang, T. Wang, P. Zhang, J. Zhang, A. Li and J. Gong, *J. Am. Chem. Soc.*, 2015, **137**, 8356-8359.
2. B. J. K. Holmberg, B. Kronberg and B. Lindman, *Surfactant and Polymers in Aqueous Solution*, John Wiley & Sons, England, 2nd edn, 2003.
3. E. Junquera, R. Arranz and E. Aicart, *Langmuir*, 2004, **20**, 6619-6625.
4. K. Kita-Tokarczyk, J. Grumelard, T. Haefele and W. Meier, *Polymer*, 2005, **46**, 3540-3563.
5. C. Huang, D. Quinn, Y. Sadovsky, S. Suresh and K. J. Hsia, *Proc. Natl. Acad. Sci. USA*, 2017, **114**, 2910-2915.
6. H. Xu and W. Wang, *Angew. Chem. Int. Ed.*, 2007, **46**, 1489-1492.
7. L. Yu, H. Hu, H. B. Wu and X. W. Lou, *Adv. Mater.*, 2017, **29**.
8. T. Wang, Y. Wei, X. Chang, C. Li, A. Li, S. Liu, J. Zhang and J. Gong, *Appl. Catal. B: Environ.*, 2018, **226**, 31-37.
9. A. Adan-Mas, T. M. Silva, L. Guerlou-Demourgues and M. F. Montemor, *Electrochim. Acta*, 2018, **289**, 47-55.
10. B. Li, G. Tan, M. Wang, D. Zhang, M. Dang, L. Lv, H. Ren, A. Xia, Y. Liu and W. Liu, *Appl. Surf. Sci.*, 2020, **511**, 145534.
11. A. Li, X. Chang, Z. Huang, C. Li, Y. Wei, L. Zhang, T. Wang and J. Gong, *Angew. Chem. Int. Ed.*, 2016, **55**, 13734-13738.
12. R. Li, F. Zhang, D. Wang, J. Yang, M. Li, J. Zhu, X. Zhou, H. Han and C. Li, *Nat. Commun.*, 2013, **4**, 1432.
13. A. Li, T. Wang, X. Chang, W. Cai, P. Zhang, J. Zhang and J. Gong, *Chem. Sci.*, 2016, **7**, 890-895.
14. A. Li, W. Zhu, C. Li, T. Wang and J. Gong, *Chem. Soc. Rev.*, 2019, **48**, 1874-1907.